J. Straub and S. Schneider

Transient Convection caused by Acceleration Disturbances*

Transient convection caused by acceleration disturbances is investigated in a fluid-filled cylinder differentially heated at its end walls. The influence of the fluid properties is considered by using silicon, air, water and glycerin as test fluids, thus a range of Prandtl numbers of four decades from 10^{-2} to 10^{2} is covered. A three-dimensional numerical code was developed, by this means the effects of the angle between the temperature gradient in the cylinder and the gravity vector could be investigated. The initial conditions in the liquid are no motion due to low gravity, and a linear temperature profile between the heated bottom and the cooled top walls of the enclosure caused by pure conduction is supposed. Several acceleration disturbances, such as step pulse, single rectangular and sinusoidal pulse and series of pulses of various amplitude, shape, and duration expressed by modified Rayleigh and Fourier numbers (Ra and Fo*) were examined. For the test of the numerical code, the Rayleigh-Bénard problem was studied for cylinders of various aspect ratios. With these results general statements can be made about the influence of acceleration disturbances on convection for material processing under microgravity, and this may help to interpret inhomogeneities in performed experiments and to avoid them in future, as well.*

1 Introduction

Since material science experiments have been performed in a microgravity environment, a lively discussion about the influence of acceleration disturbances on material specimens has come up, and is still going on. Such interferences of the microgravity environment induce convection in liquids, when they are differentially heated in their process containers. This convection might, in turn, cause inhomogeneities in the solid material or in the crystal structure, if such g-jitter perturbations occur during the solidification process. On the earth the influence of such disturbances cannot be studied, because an experimental simulation of a low gravity environment is only possible in space vehicles, or for a short period of time, in sounding rockets. Therefore the onset of convection and the development of the transient flow field under g-jitter disturbances can only be studied by means of numerical simulations, which may help to interpret and plan space experiments, although no prediction of the inhomogeneities to be expected in the solid material can be made. For the simulation of the effects of g-jitter disturbances in liquids, we developed a numerical code to calculate three-dimensional laminar natural convection in a cylinder differentially heated at its end walls using the experience of many years in numerically solving thermo-fluid-dynamic problems [1–4]. In former papers [5, 6] we reported in excerpts about this study, which was concluded in 1990 [7], whereas a summary of the most important aspects of g-jitter effects is presented in this paper.

In [5] and [6], and in detail in [7], a review is given on former works on this problem [8–14]. Most of these papers contain analytical solutions or two-dimensional approximations, in which the influence of the cylinder's angle of inclination towards the gravity vector could not be considered. Due to the lack of space here, we refer to the literature for a complete overview.

2 Acceleration Disturbances

Before the numerical analysis is presented, the question of the gravity disturbances to be expected during a space mission is discussed. A general analysis of the microgravity environment of an earth-orbiting system was presented by *Hamacher* et al. [15], while the characteristic features of gravity interferences recorded during the D1-mission are carefully evaluated by *Hamacher* et al. [16], and are well-known from our own observations and recordings on MEDEA HPT during this mission.

Both external and internal forces may give rise to acceleration disturbances. The external forces are caused by operational activities, such as thruster firings for altitude control. The main direction of such disturbances is along the axis of the orbiter vehicle with highest spikes of $60 \cdot 10^{-3}\, g_0$. The internal forces result from mass allocation inside the space vehicle due to mechanical motions of experimental facilities and crew activities. Impulses caused by these internal forces are always compensated by impulses of the same size in opposite direction with a time delay corresponding to the resonant frequency of the experimental module overlapped by the natural frequency of the Spacelab module in its suspension. Typical spikes have

* This paper is the complete version of the paper "Transient Convection caused by Acceleration Disturbances" by J. Straub and S. Schneider published in Microgravity sci. technol. IV, 2, pp. 156–157 (1991), as extended abstract of a contribution for the IUTAM-Symposium on Microgravity Fluid Mechanics, Bremen 1991.

Mail address: Prof. Dr-Ing.habil. Johannes Straub, Lehrstuhl A für Thermodynamik, Technical University Müchen, Arcisstrasse 21, D-W-8000 Müchen 2, Germany.

amplitudes of less than $10 \cdot 10^{-3} g_0$, but they are often random in their direction. In quiet phases, peaks of the resulting gravity vector are recorded to be $0.2 \cdot 10^{-3} g_0$ in maximum.

Considering the above facts, it is obvious that a general prediction of the influence of gravity disturbances cannot be given. Firstly, they depend on the space vehicle and the mission itself; most of the disturbances are random in direction, amplitude, and time of their occurring. For special sensitive experiments, quiet phases can be arranged, however, not for the complete period of a manned mission. Secondly, the experiment itself, the geometry, the size of the temperature gradient in the liquid, the direction of the acceleration vector with respect to the temperature gradient, and the properties of the fluid are of considerable importance. For each sensitive experiment, a separate analysis should therefore be made taking into account all the influence factors mentioned. Here a more general study is presented, in which the shape, the amplitude, the frequency and the direction of the acceleration pulses, the properties of the liquid, and the aspect ratio of the cylindrical enclosure are considered as parameters.

3 Theoretical Approach

3.1 Physical and Mathematical Models

The problem under consideration is sketched in fig. 1. The transient three-dimensional buoyancy-driven flow in a cylindrical enclosure filled with gas or liquid is governed by the following equations, when work of compression and viscous dissipation are neglected:

- Equation of continuity:

$$\frac{\mathscr{D}\varrho}{\mathscr{D}t} = -\varrho(\nabla \cdot \boldsymbol{v}) \tag{1}$$

- Equation of motion:

$$\varrho \cdot \frac{\mathscr{D}\boldsymbol{v}}{\mathscr{D}t} = -\nabla p + \nabla \bar{\bar{\tau}} + \varrho \boldsymbol{g} \tag{2}$$

- Equation of energy:

$$\varrho c_p \cdot \frac{\mathscr{D}T}{\mathscr{D}t} = \nabla(\lambda \nabla T) \tag{3}$$

The following differential operators are employed:

$$\frac{\mathscr{D}}{\mathscr{D}t} = \frac{\partial}{\partial t} + v_r \frac{\partial}{\partial r} + \frac{v_\varphi}{r} \frac{\partial}{\partial \varphi} + v_z \frac{\partial}{\partial z}$$

$$\nabla = \frac{1}{r} \frac{\partial}{\partial r} r + \frac{1}{r} \frac{\partial}{\partial \varphi} + \frac{\partial}{\partial z}. \tag{4}$$

We assume no-slip conditions at all rigid walls:

$$\boldsymbol{v}|_{\text{wall}} = \boldsymbol{0} \tag{5}$$

The thermal boundary conditions are isothermal top and bottom walls:

$$T(r, \varphi, 0) = T_{hot},$$

$$T(r, \varphi, H) = T_{cold}. \tag{6}$$

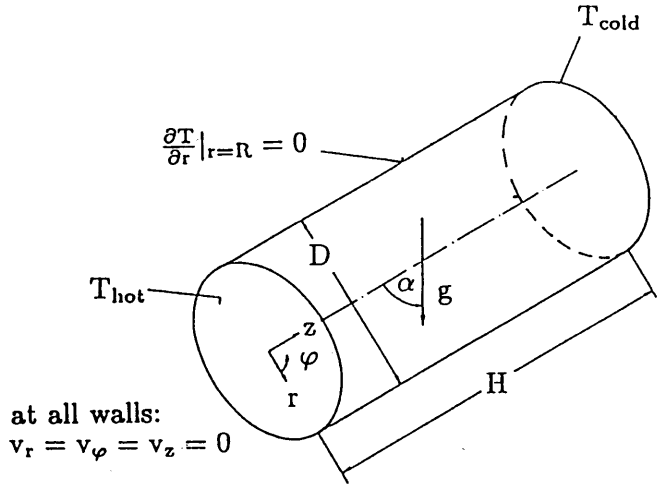

Fig. 1. Schematic diagram of the enclosure with boundary conditions and gravity vector

Furthermore, a perfectly insulated lateral wall is assumed:

$$\left.\frac{\partial T}{\partial r}\right|_{r=R} = 0. \tag{7}$$

For gases the equation of state for an ideal gas applies:

$$\varrho(T) = \frac{p}{R_0 T} \tag{8}$$

while the density of the liquids is calculated from:

$$\varrho(T) = \frac{\varrho_0}{1 + \beta_p (T - T_0)}. \tag{9}$$

The aspect ratio of height to diameter A, the inclination angle α of the cylinder's axis towards the direction of the gravity field, the Prandtl and Rayleigh numbers can independently be varied. The following scales for obtaining dimensionless quantities are employed:

- Rayleigh number:

$$Ra = \frac{g \beta_p D^3 (T_{hot} - T_{cold})}{va} \tag{10}$$

- Modified Rayleigh number of pulse amplitude:

$$Ra^* = \frac{g^* \beta_p D^3 (T_{hot} - T_{cold})}{va} \tag{11}$$

- Prandtl number:

$$Pr = \frac{v}{a} \tag{12}$$

- Fourier number:

$$Fo = \frac{ta}{D^2} \tag{13}$$

- Modified Fourier number of pulse duration or oscillation period:

$$Fo^* = \frac{\hat{t}a}{D^2} \tag{14}$$

- Dimensionless velocity:

$$v^* = \frac{vD}{a} \tag{15}$$

- Dimensionless frequency:

$$f^* = \frac{fD^2}{a}. \tag{16}$$

3.2 Method of Solution

For the study of transient laminar natural convection in a cylinder by a three-dimensional calculation, the numerical code is based upon a finite-volume method with explicit time steps and a semi-iterative pressure-velocity correction (SIMPLE) [17]. The conservation equations for mass, momentum, and energy (1)–(3) are discretized by using an equidistant mesh ($\Delta r = const.$, $\Delta\varphi = const.$, $\Delta z = const.$).

The algebraic equations are formulated in terms of primitive variables (v_r, v_φ, v_z, p, T). Temperature and pressure are defined in the center of the finite volumes. The velocities are calculated for points on the faces of the control volumes by employing a "staggered grid". All properties are constant, except density, which is assumed to depend on temperature only. The density of air is calculated from eq. (8), while the density of the liquids is indirectly proportional to their temperature in eq. (9). Further computational details are given in [5–7].

For every time-step, the flow field is calculated, and the maximum velocity is determined in order to describe the intensity of the fluid motion. Even if location and direction of the maximum velocity vary, its magnitude is an upper limit for all velocities in the fluid, and it is used in the graphs to characterize the intensity of the flow. In a horizontal cylinder the fluid moves upward at the hot wall to stream down again at the cold wall forming a single roll. For a cylinder of $A = 1$, the velocities in the vicinity of the hot and cold walls are of the same magnitude as the ones adjacent to the lateral wall. Thus, even if the maximum velocity is observed adjacent to the lateral wall, it describes the velocities near the hot and cold walls, as well.

3.3 Fluid Properties

To consider the influence of the properties, four different fluids are used for the calculation: silicon, air, water, and glycerin. The properties are given in table 1. In thermofluid-dynamic problems, the Prandtl number is an important property, which is varied with the selected fluids over about four decades from 10^{-2} to 10^2. It should be mentioned that for the low-Prandtl number fluid silicon, the calculation consumes much more CPU time than for the other fluids.

4 Results

4.1 Rayleigh-Bénard Problem for Various Aspect Ratios

To test the sensitivity of the numerical code, the unstable density stratification was examined in a Rayleigh-Bénard problem. Moreover, the critical Rayleigh number was determined for various aspect ratios A of a cylinder filled with air as test fluid. To obtain the critical Rayleigh number, the onset of convection was initiated by a small temporary perturbation. The initial conditions for this case were no motion in the fluid, a linear temperature distribution from bottom to top with the higher temperature at the bottom, and a hydrostatic pressure profile according to earth gravity along the vertical z-axis. The perturbation was activated by inclining the cylinder for the duration of one time step by an angle of only 0.1° from the vertical position for aspect ratios $A \geq 1$. For aspect ratios $A \leq 1/2$, the disturbance was brought about by an initial hot spot in the center of the bottom wall during the first time step of the calculation. By this method, stable flow modes were induced, which was for $A \geq 1$ the non-axisymmetric roll mode with fluid moving upward on one side and flowing downward on the other one; for $A \leq 1/2$ an axisymmetric toroidal flow mode prevailed, despite the non-axisymmetric activation. Using this technique, it could be guaranteed that the stable flow modes were activated.

Table 1. Properties of the investigated fluids

fluid	silicon	air ($p = 1$ bar)	water	glycerin
Pr	0.023	0.71	7.0	134.9
ν [10^{-6} m^2 s^{-1}]	0.3	15.1	1.0	11.9
a [10^{-6} m^2 s^{-1}]	13.0	21.3	0.14	0.088
c_p [J kg^{-1} K^{-1}]	1,047.96	1,005	4,183	2,430
ϱ_0 [kg m^{-3}]	2,500	1.2045	998.2	1,260.4
T_0 [K]	1,690	293	293	293
β_p [10^{-4} K^{-1}]	1.43	34.13	1.8	4.9

It is interesting to note that our computer code comprises all the physics necessary to fully describe the stability of the flow (fig. 2). If $Ra < Ra_{crit}$, the initial flow is damped out after its activation by the perturbation. However, if $Ra > Ra_{crit}$, the maximum velocity in the flow field in-

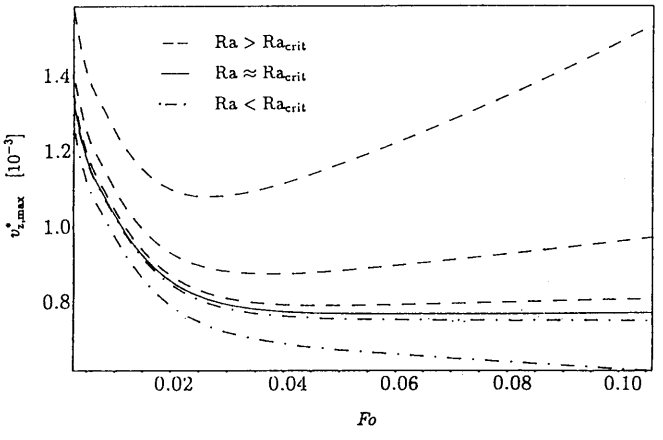

Fig. 2. Transient development of the maximum axial velocity after an initial perturbation in the Rayleigh-Bénard problem

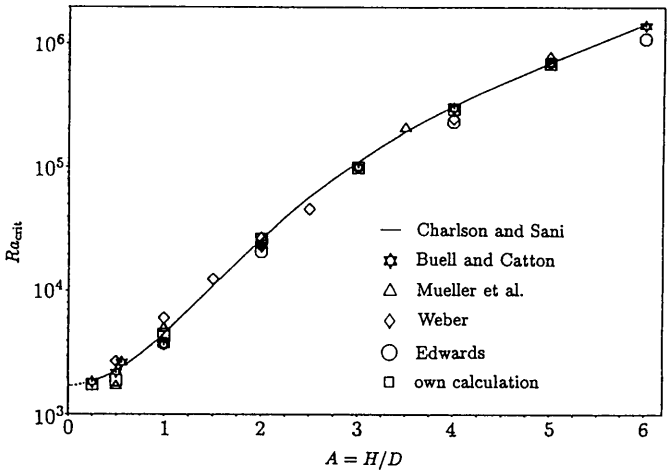

Fig. 3. Dependence of the critical Rayleigh number on the aspect ratio of the cylinder

creases again, after the initial flow due to the perturbation has faded away, and reaches a finite steady-state value after some time. Only for the case of the critical Rayleigh number, a steady flow develops after the decay of the initial disturbance with small velocities and the characteristic $dv^*/dFo = 0$. In fig. 3 the calculated critical Rayleigh numbers are compared with the theoretical results of *Charlson* and *Sani* [18], *Buell* and *Catton* [19], and *Edwards* [20], and with the experimental results of *Mueller* et al. [21], and *Weber* [22]. For $A \to 0$, the critical Rayleigh number approaches the classical value of $Ra_{crit} = 1707.8$ for the infinite horizontal fluid layer.

4.2 Direction of the Gravity Vector

The influence of the angle α between the temperature gradient and the gravity vector is an important parameter for the onset of convection, and is investigated for a cylinder of $A = 1$. The initial conditions are a linear temperature profile in axial direction and no motion in the fluid corresponding to $g = 0$ and $Ra = 0$, respectively. For $t = 0$ or

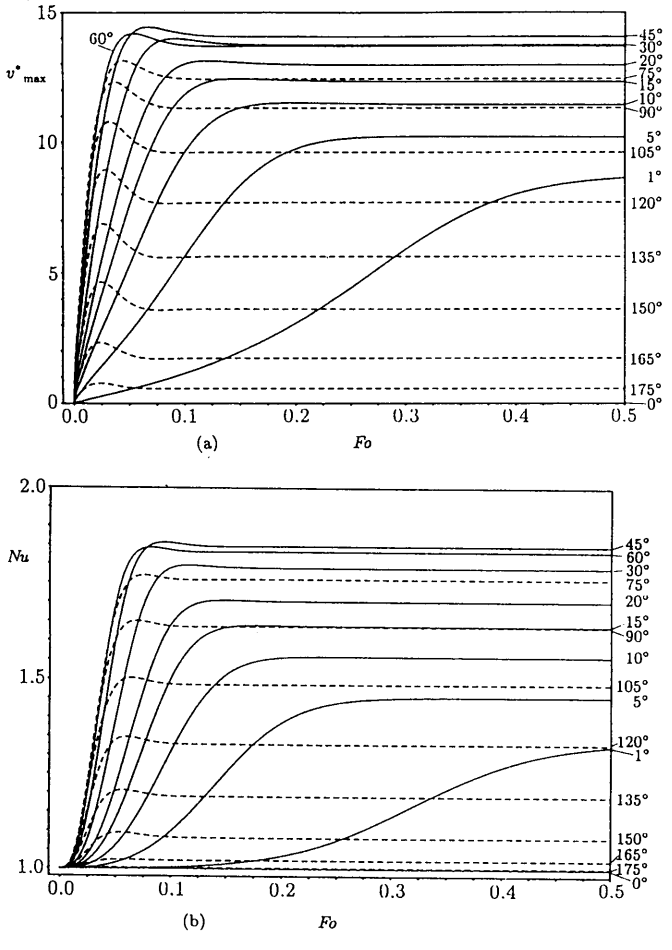

Fig. 4. Intensity of the flow field v^*_{max} (a) and averaged Nusselt number Nu (b) dependent on the dimensionless time Fo for different angles on inclination for air (Ra = 5,000)*

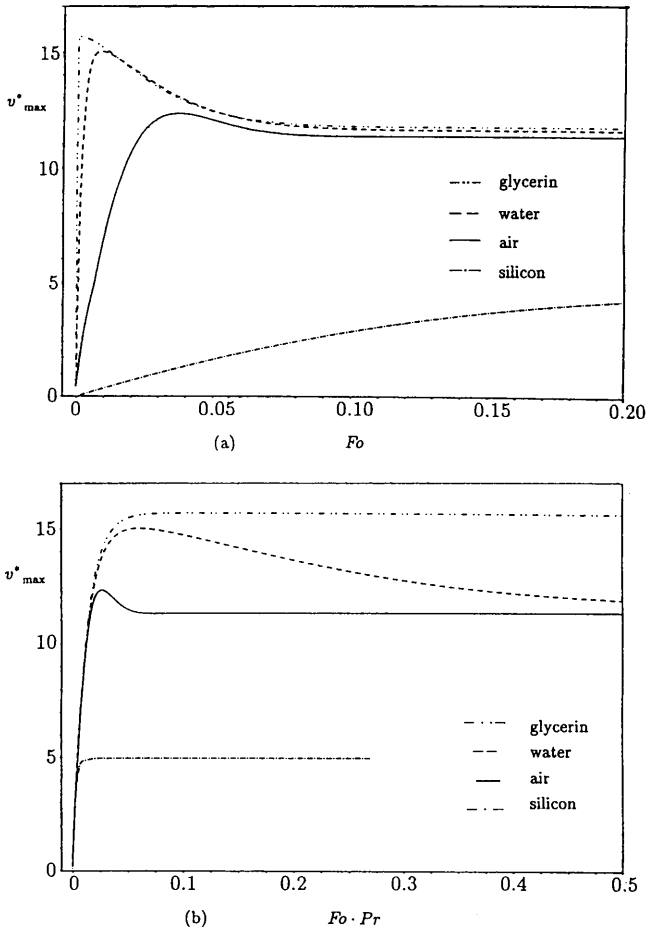

Fig. 5. Transient development of the maximum velocity for the liquids investigated (a), using a different time scale (b) ($\alpha = 90°$, Ra = 5,000)*

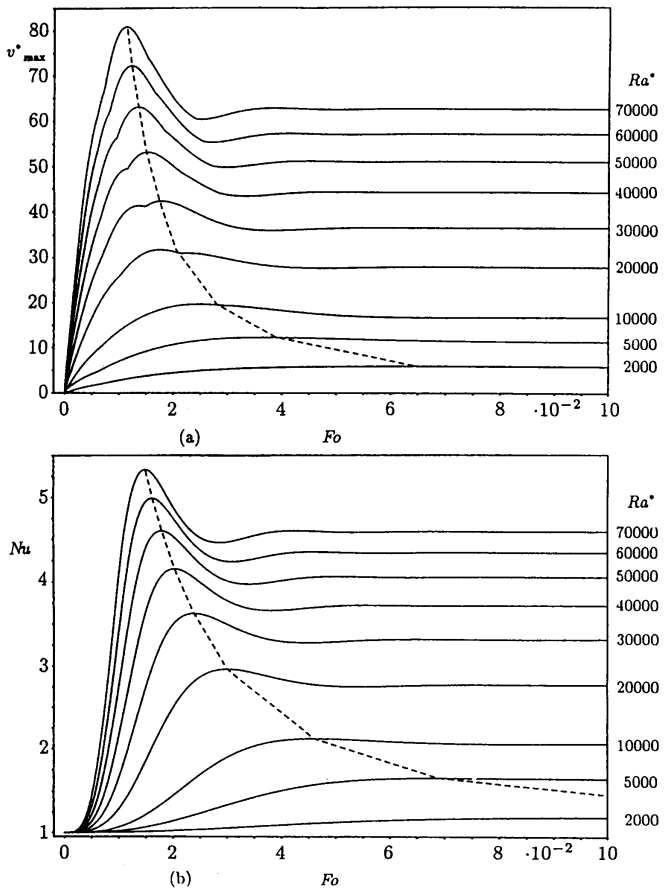

Fig. 6. Transient development of the flow field (a) and the heat transfer (b) for different amplitudes Ra of the step pulse (α = 90°, air)*

$Fo = 0$, a sudden change of the gravity level to g^*, characterized by $Ra^* = 5{,}000$, was induced. This value was kept constant, until steady-state flow was established. The angle $\alpha = 0°$ represents a gravity vector of the same orientation as the temperature gradient. The density stratification is unstable for $\alpha \geq 0°$, because the bottom is heated, whereas $\alpha = 180°$ describes a stable stratification resulting only from heat conduction.

The calculations were performed for air, water, glycerin, and silicon, although only few results are presented here. In fig. 4a the development of the maximum dimensionless velocity is plotted versus the dimensionless time, the Fourier number. For small angles of inclination, the reaction of the flow is slow, increasing with α and overshooting at higher angles. Maximum flow and heat transfer (fig. 4) are achieved for $\alpha = 45°$. It is remarkable that, in the beginning, the maximum velocity is identical for both the inclinations α and $180° - \alpha$. The development of the flow and the heat transfer is similar for water, glycerin, and silicon. For silicon, with its low Prandtl number, both the maximum velocity and the heat transfer are shifted to an angle between 60° and 75°. The steady-state averaged Nusselt number for $Ra^* = 5{,}000$ is increased from unity, representing pure heat conduction, to 1.7 for air, 1.6 for water, and 1.21 for silicon.

In fig. 5a the onset of convection is sketched for the investigated liquids for $\alpha = 90°$ and a gravity step of infinite duration Fo^* and of amplitude $Ra^* = 5{,}000$. The overshooting of the maximum velocity declines with decreasing Prandtl number. Glycerin, water, and air obtain a steady-state flow within a time of $Fo < 0.1$. The flow field of silicon reacts with some delay, no overshooting is observed, and steady-state conditions are reached one order of the dimensionless time later than with the other fluids. If $Fo \cdot Pr = t \cdot v/D^2$ is used as a new dimensionless time scale in fig. 5b, the initial maximum velocities coincide with each other on one curve for the four liquids investigated. This means that, in the early stage, the development of the flow is dominated by the fluid's viscosity.

The influence of the gravity step, expressed by the Rayleigh number, is demonstrated in fig. 6 for air and $\alpha = 90°$. With an increasing Rayleigh number, the flow reacts faster, the maximum velocity, the overshooting, and the Nusselt number increase. The peak value of the velocities $v^*_{max,peak}$, which is illustrated as a dashed line, is proportional to approximately $Fo^{-1.52}$.

A comparison between water, air, and silicon for gravity steps of $Ra^* = 5{,}000$ and $Ra^* = 20{,}000$ is given in fig. 7. The steady-state velocity ($Fo > 0.1$) and the overshooting increase with both the Prandtl and Rayleigh numbers.

4.3 Single Rectangular Pulse

Single rectangular pulses of various amplitude and different duration, expressed by the modified Rayleigh number Ra^* and the modified Fourier number Fo^*, respectively, are applied perpendicular to the temperature gradient to an air-filled ($Pr = 0.7$) cylinder ($\alpha = 90°$). The initial conditions are the same as above, no motion due to low gravity, and a linear temperature profile between the differentially heated

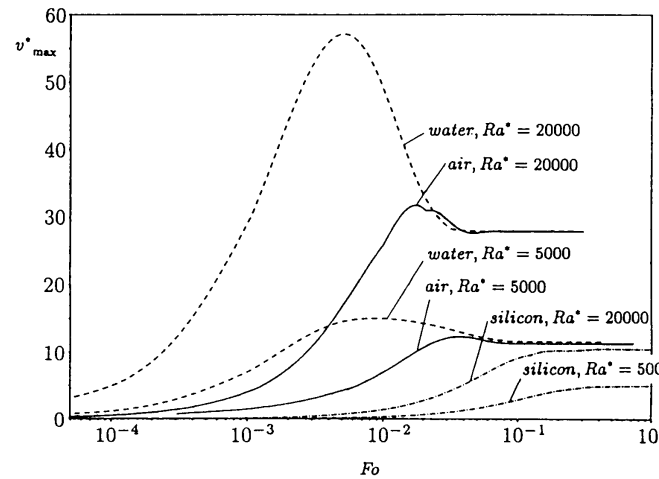

Fig. 7. Comparison of the behaviour of the investigated fluids towards step pulses of different amplitude Ra (α = 90°)*

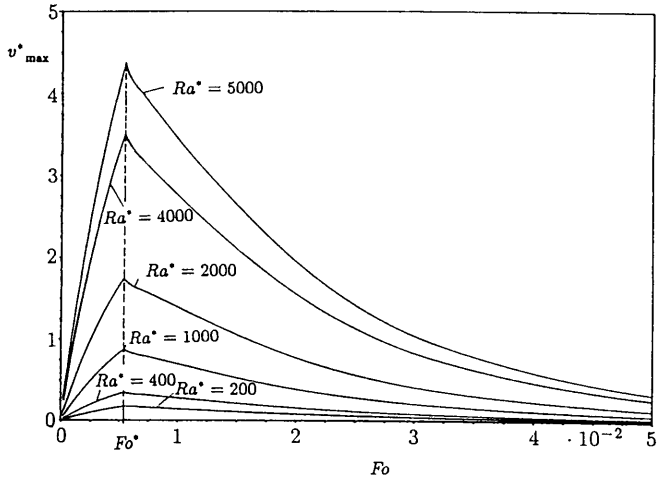

Fig. 8. Maximum velocity v^*_{max} vs dimensionless time Fo for rectangular pulses of different amplitude Ra ($\alpha = 90°$, air, $Fo^* = 5.5 \cdot 10^{-3}$)*

end walls. In fig. 8 the increase of the dimensionless maximum velocity is shown for the duration of the gravity pulse of $Fo^* = 5.5 \cdot 10^{-3}$. The peak velocity depends on the intensity Ra^*, and the duration Fo^* of the pulse, and on the aspect ratio A. The ratio of the peak velocity to the amplitude of the pulse is constant for a certain aspect ratio:

$$\frac{v^*_{max,peak}}{Ra^*} = const. \tag{17}$$

Thus all graphs of fig. 8 coincide on one curve, if this ratio is used for the ordinate. The convective flow fades away exponentially and independently of the amplitude Ra^*, after the pulse has been applied:

$$\frac{v^*_{max}}{v^*_{max,peak}} = \exp\left(\frac{Fo^* - Fo}{\tau}\right), \quad \text{for } Fo > Fo^*. \tag{18}$$

The decay constant τ depends, as shown in table 2, only on the aspect ratio A, and not on the amplitude or duration of the pulse.

Table 2. Decay constant τ in eq. (14)

A	τ
0.5	0.020
1.0	0.038
2.0	0.053
5.0	0.061

4.4 Single Sinusoidal Pulse

A sinusoidal gravity pulse of one period duration is exerted perpendicular to the temperature gradient of the cylindrical enclosure. The time-dependency of gravity is obtained from:

$$g(t) = g^* \cdot \sin(2\pi f \cdot t). \tag{19}$$

The amplitude of the pulse is described as before by Ra^*, and its period by Fo^* and by the dimensionless frequency:

$$f^* = \frac{1}{Fo^*}. \tag{20}$$

A cycle of oscillation comprises a positive and a negative amplitude of the same size. The dimensionless amplitude can also be expressed as a function of time:

$$Ra(Fo) = Ra^* \cdot \sin\left(2\pi \cdot \frac{Fo}{Fo^*}\right). \tag{21}$$

Fig. 9 shows the maximum velocity for water ($Pr = 7.0$) and an aspect ratio of $A = 1$ for different amplitudes Ra^*. The maximum velocity depends on the amplitude Ra^*, and decreases rapidly after a certain cut-off frequency of $f^* \approx 70$ has been exceeded. It is interesting that an over-

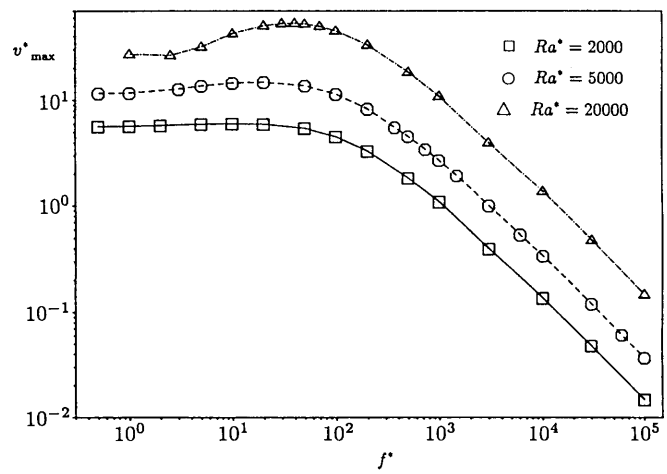

Fig. 9. Maximum velocity v^*_{max} vs dimensionless frequency f^* for sinusoidal pulses of different amplitude Ra ($\alpha = 90°$, water)*

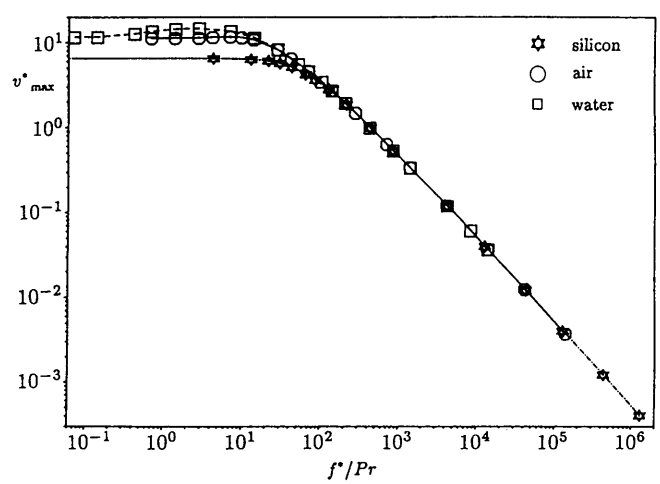

Fig. 10. Comparison of the maximum velocity v^*_{max} of different fluids with f^*/Pr as a new time scale for sinusoidal pulses of $Ra^* = 5{,}000$ ($\alpha = 90°$)

shooting of the velocity appears at higher amplitudes for frequencies $f^* > 1$. The overshooting can be explained as a resonance between the excitation and the fluid motion.

The decay rate of the velocity with increasing frequency is independent of the fluid, and one curve is obtained for the different fluids, if f^*/Pr is chosen for the abscissa in fig. 10. Furthermore, the magnitude of the velocities at very low frequencies seems to be independent of the fluid for $Pr \geq 1$ and lower values of Ra^*, while it is significantly smaller for silicon. The value for the cut-off frequency depends linearly on the Prandtl number, and is $f^*/Pr \approx 10$.

4.5 Periodical Rectangular Pulse

As before, the gravity pulses are applied perpendicular to the temperature gradient ($\alpha = 90°$), and the frequency f^* is defined as in eq. (20) for the case of the single sinusoidal pulse with positive and negative amplitude; its shape is, however, rectangular. The maximum velocities are registered, as soon as a steady-state oscillation has been achieved.

For low frequencies, steady-state velocities are obtained after each reversal of the gravity step, they are approximately the same as for the single step described in sect. 4.3. For higher frequencies, the velocities are about 50 % smaller than in the case of the single pulse of equivalent duration. This is obvious, because after each step the flow is just in opposite direction to the excited new pulse, and the inertia of the flow must first be overcome, before the flow is converted in the direction of the new pulse. The velocity is decreasing for higher frequencies, while the cut-off frequency is approximately the same one as mentioned before. If the ratio of the frequency to the Prandtl number is employed, the decay of the maximum velocity coincides on one curve for the various fluids as in sect. 4.4. (fig. 11).

The ratio

$$\frac{f^*}{Pr} = f \cdot \frac{D^2}{\nu} \tag{22}$$

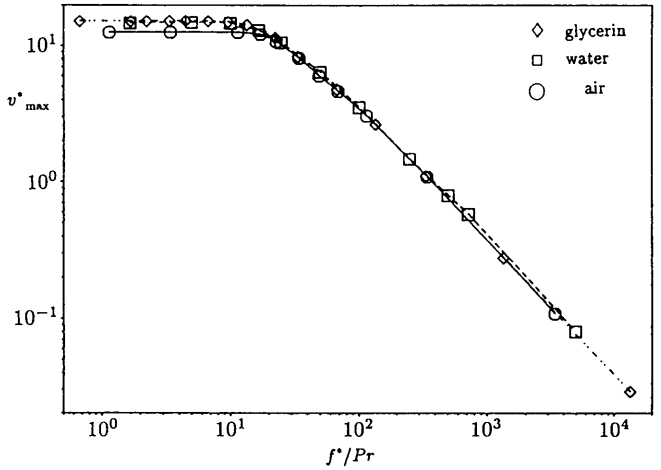

Fig. 11. Comparison of the maximum velocity v^*_{max} of different fluids with f^*/Pr as a new time scale for periodical rectangular pulses of $Ra^* = 5{,}000$ ($\alpha = 90°$)

represents a dimensionless frequency, now defined with the kinematic viscosity ν instead of the thermal diffusivity a in eq. (16). That means that for $f^*/Pr > 10$, only the viscous forces dominate the flow, while the velocity still depends on the amplitude Ra^* for lower frequencies.

5 Conclusion

In this numerical study the transient convective flow caused by various gravity perturbations is investigated in a cylindrical enclosure differentially heated at its end walls. The initial conditions are a linear temperature profile between bottom and top walls, no motion in the fluid corresponding to low gravity, and a constant pressure distribution. In terms of the dimensionless numbers Ra^*, Fo, Pr, and the dimensionless velocity v^*_{max} and frequency f^*, general results are presented. With our three-dimensional code, the influence of the angle of inclination α between the gravity vector and the temperature gradient could be examined. Although these results are strictly valid only in the range of the investigated parameters, more general conclusions can be drawn, if convection in a microgravity environment caused by g-jitter perturbations is to be avoided:

- Accelerations perpendicular to the temperature gradient induce greater velocities than those in parallel direction, and the reaction is much faster. Experimental facilities in an orbital lab should be orientated in a way that the expected transient accelerations are parallel to the temperature gradient in the fluid.
- The effects of residual acceleration can be reduced, if the experimental set-up is aligned in such a manner that the acceleration vector acts in opposite direction of the temperature gradient.
- Disturbances of high frequency are insignificant.
- The maximum velocities are proportional to the Rayleigh number, i.e. the velocities increase for a given acceleration with the third power of the dimension in the direction of the acceleration vector.
- Fluids with a small Prandtl number $Pr \ll 1$ (e.g. liquid silicon) are less sensitive to disturbances than fluids with higher Prandtl numbers Pr.
- In the range of frequencies below the cut-off frequency $f^*/Pr \approx 10$, a strong overshooting of the velocity occurs with increasing amplitudes Ra^* and increasing Prandtl number.
- A periodical series of positive and negative accelerations induce lower velocities than a single pulse of the same duration for $f^*/Pr > 10$.
- The geometrical shape, the aspect ratio, and the thermal boundary condition on the lateral wall of the cylinder are not as significant to acceleration disturbances as might be supposed.
- Characteristic features of the transient flow can be studied by examining the flow caused by a single acceleration pulse.
- The velocities caused by superimposed acceleration pulses can be estimated by overlapping different velocity graphs, as the velocities are directly proportional to the amplitude of the interference.

It is obvious that only general statements and recommendations for planning space experiments can be derived from these results. For very sensitive experiments, special three-dimensional calculations have to be performed, where all parameters of influence can be considered.

List of Symbols

a	thermal diffusivity
A	aspect ratio $= H/D$
c_p	isobaric specific heat capacity
D	diameter of the cylinder
$\mathscr{D}$	substantial derivative
f	frequency of a pulse
f^*	dimensionless frequency
Fo	Fourier number
Fo^*	modified Fourier number
$\boldsymbol{g}$	vector of variable gravitational acceleration $= (g_r, g_\varphi, g_z)^T$
g_0	gravity on earth
H	height of the cylinder
Nu	Nusselt number
p	pressure
Pr	Prandtl number
r	radial coordinate
Ra	Rayleigh number
Ra^*	modified Rayleigh number
t	time
$\hat{t}$	pulse duration or period
T	temperature
T_0	reference temperature for density
$\boldsymbol{v}$	vector of velocity $= (v_r, v_\varphi, v_z)^T$
v^*	dimensionless velocity
z	axial coordinate
α	angle between temperature gradient and vector of gravity
β_p	isobaric expansion coefficient $= -\frac{1}{\varrho}\left(\frac{\partial \varrho}{\partial T}\right)_p$
Δ	increment
η	dynamic viscosity
λ	thermal conductivity
ν	kinematic viscosity
ϱ	density
ϱ_0	reference value for the density
φ	azimuthal coordinate
τ	decay constant
$\bar{\bar{\tau}}$	stress tensor
∇	nabla operator

subscripts:

cold	cold wall
crit	critical value
hot	hot wall
max	maximum value
peak	peak value
wall	value on the wall
0	reference value

Acknowledgement

We gratefully acknowledge that the second author was financially supported for two years by a scholarship for the promotion of young scientists from the Bavarian Government, and for additional two years by the Loschge Foundation of the Technical University of Munich.

References

1 *Kueblbeck, K., Merker, G.P., Straub, J.:* Advanced Numerical Calculation of Two-Dimensional Time-Dependent Free Convection in Cavities. Int. J. Heat Mass Transfer 23 (1980) 203.
2 *Kueblbeck, K.:* Laminare und turbulente Ausbreitungsvorgaenge infolge freier und erzwungener Konvektion. Doctoral Thesis, Technical University of Munich (1981).
3 *Stoll, J.:* Wärmeübertragung und Filmkühlung in kompressibler Düsenströmung. Doctoral Thesis, Technical University of Munich (1987).
4 *Heiss, A.:* Numerische und experimentelle Untersuchungen der laminaren und turbulenten Konvektion in einem geschlossenen Behälter. Doctoral Thesis, Technical University of Munich (1987).
5 *Schneider, S., Heiss, T., Straub, J.:* Natural Convection in a Cylinder caused by Gravitational Interferences: A Three-Dimensional Numerical Calculation. Proc. Intern. Symp. on Thermal Problems in Space-Based Systems, ASME HTD 83, Dobran, F., Imber, M. (eds.). New York: ASME (1987) 77.
6 *Schneider, S., Straub, J.:* Influence of the Prandtl Number on Laminar Natural Convection in a Cylinder caused by g-jitter. J. Crystal Growth 97 (1989) 235.
7 *Schneider, S.:* Laminare freie Konvektion in einem Zylinder bei konstanter und zeitveränderlicher Schwerkraft (g-jitter). Doctoral Thesis, Technical University of Munich (1990).
8 *Elder, J. W.:* The Temporal Development of a Model for High Rayleigh Number Convection. J. Fluid Mechanics 35 (1969) 417.
9 *Foster, T. D.:* The Effect of Initial Conditions and Lateral Boundaries on Convection. J. Fluid Mechanics 37 (1969) 81.
10 *Gresho, P. M., Sani, R. L.:* The Effects of Gravity Modulation on the Stability of a Heated Fluid Layer. J. Fluid Mechanics 40 (1970) 783.
11 *Monti, R., Langbein, D., Favier, J. J.:* Influence of Residual Accelerations on Fluid Physics and Materials Science in Space. Walter, H. U. (ed.): Fluid Sciences and Material Sciences in Space. Berlin, Heidelberg, New York, London, Paris, Tokyo: Springer Verlag (1987) 637.
12 *Griffin, P. R., Motakef, S.:* Analysis of the Fluid Dynamics and Heat Transfer during Micro-Gravity Bridgman-Stockbarger Growth of Semiconductors in Steady Periodic Gravitational Fields. ASME Paper 87-WA/HT-1. New York: ASME (1987).
13 *Kirchartz, K. R.:* Zeitabhängige Konvektion bei verminderter Gravitation. Spacelab Nutzungen, Status-Seminar 1982 des Bundesministerium für Forschung und Technologie (1982) 43–59, also in: Z. Flugwiss. Weltraumforsch. 6 (1982) 300.
14 *Kirchartz, K. R., Oertel, H. jr., Zierep, J.:* Time-Dependent Convection. Zierep, J., Oertel, H. jr. (eds.) Convective Transport and Instability Phenomena. Karlsruhe: Verlag G. Braun (1982) 101.
15 *Hamacher, H., Fitton, B., Kingdon, J.:* The Environment of Earth-Orbiting Systems. Walter, H. U. (ed.): Fluid Sciences and Material Sciences in Space. Berlin, Heidelberg, New York, London, Paris, Tokyo: Springer Verlag (1987) 1.
16 *Hamacher, H., Jilg, J., Merbold, U.:* Analysis of Microgravity Measurements Performed during D1. Proc. 6th European Symposium on Material Sciences under Microgravity Conditions, Bordeaux, France (1986) ESA SP-256 413.
17 *Patankar, S. V.:* Numerical Heat Transfer and Fluid Flow. Washington, London: Hemisphere Publishing Corporation (1980).
18 *Charlson, G. S., Sani, R. L.:* On Thermoconvective Instability in a Bounded Cylindrical Fluid Layer. Int. J. Heat Mass Transfer 14 (1971) 2157.
19 *Buell, J. C., Catton, I.:* The Effect of Wall Conduction on the Stability of a Fluid in a Right Circular Cylinder Heated from below. J. Heat Transfer 105 (1983) 255.
20 *Edwards, D. K.:* Suppression of Cellular Convection by Lateral Walls. J. Heat Transfer 91 (1969) 145.
21 *Mueller, G., Neumann, G., Weber, W.:* Natural Convection in Vertical Bridgman Configurations. J. Crystal Growth 70 (1984) 78.
22 *Weber, W.:* Untersuchung der thermokapillaren Auftriebskonvektion in Modellsystemen zur Kristallzüchtung bei normaler und erhöhter Schwerkraft. Doctoral Thesis, University of Erlangen-Nürnberg (1988).